Contents lists available at ScienceDirect

Electrochimica Acta

journal homepage: http://ees.elsevier.com

Towards an optimized hybrid electrochemical capacitor in iodide based aqueous redox-electrolyte: Shift of equilibrium potential by electrodes mass-balancing

Q. Abbas [a,*], H. Fitzek [b], V. Pavlenko [c], B. Gollas [a]

[a] Institute for Chemistry and Technology of Materials, Graz University of Technology, Stremayrgasse 9, 8010, Graz, Austria
[b] Graz Centre for Electron Microscopy, Steyrergasse 17, 8010, Graz, Austria
[c] Al-Farabi Kazakh National University, 71 al-Farabi Ave, 050040, Almaty, Kazakhstan

ARTICLE INFO

Article history:
Received 11 November 2019
Received in revised form 21 January 2020
Accepted 24 January 2020
Available online xxx

Keywords
Equilibrium potential
Hybrid capacitor
Aqueous redox electrolyte
Polyiodides
Mass-balancing
Raman spectroscopy

ABSTRACT

Considering the cost-effectiveness, safety, and environmental friendliness for energy storage and delivery at high rates, hybrid electrochemical capacitors in aqueous electrolytes containing redox-active species are attractive alternatives to expensive organic electrolyte based electric double-layer capacitors (EDLCs). Here, the influence of electrode mass-balancing on the equilibrium potential of hybrid cells in aqueous sodium nitrate + sodium iodide (5 mol L^{-1} $NaNO_3$ + 0.5 mol L^{-1} NaI) has been investigated. The shift of equilibrium potential determines, whether the positive electrode behaves fully battery-like (charge/discharge strictly in the iodide redox potential range) or shows a mixed battery-like and EDL capacitive behavior. With an appropriate mass-balancing of the positive and negative electrodes (mass ratio = 1:2), the equilibrium potential shows a negligible shift during galvanostatic charge/discharge cycles at 0.5 A g^{-1}, which results in full battery-like behavior of the positive electrode. Consequently, the hybrid cell exhibits stable electrochemical performance. By contrast, an equal or higher mass of the positive compared to the negative electrode, leads to a shift of the equilibrium potential resulting in two different charge storage mechanisms at the positive electrode. As a result, the overall performance of the hybrid cell deteriorates. We show by thermogravimetric analysis and Raman spectroscopy that the formation of polyiodides (I_3^- and I_5^-) is controlled by the oxidation of iodide (I^-) anions to molecular iodine in nanoporous carbon based positive electrode, and that more polyiodides are produced, if the positive electrode operates strictly within the iodide/iodine redox potential range.

1. Introduction

In the past few decades, quest for efficient storage and delivery of electric energy has led to a remarkable research interest in cost effective systems such as electrochemical capacitors (ECs). ECs are well-known for storing energy at low power demand and releasing it in short bursts at peak power demand, for millions of times [1–9]. Owing to many advantages related to easy assembling, shipment, and disposal, ECs with aqueous electrolytes are considered sustainable alternatives to systems based on organic electrolytes. The latter are prepared with hazardous chemicals such as acetonitrile. For ECs with traditional acidic or alkaline as well as neutral aqueous electrolytes (pH ≈ 7), the assembling and components cost is low, requiring no inert atmosphere or extensive drying of the carbon electrodes [10–15]. Neutral aqueous electrolytes are beneficial in providing an extended potential range owing to the negative shift of the Nernst potential for hydrogen evolution at the negative carbon electrode [16]. This effect is provoked by an increase of the local pH during the electrochemical reduction of water, which produces hydroxyl anions (OH^-) [17–19]. Another advantage of aqueous electrolytes is their high ionic conductivity (0.1–0.5 S cm^{-1}), which helps to reduce ohmic losses via efficient transport of ions within the porous electrode materials.

A major drawback of aqueous electrolytes based on alkali sulfate or nitrate [20–22], however, is the low reachable voltage of 1.5 or 1.6 V [20–22], which results in a low specific energy of the device. Internal hybridization of two electrodes (inside a single device) with different charging mechanisms in aqueous electrolytes, is a promising strategy to compensate for the low voltage [23,24]. In such a hybridized system, one electrode exhibits a large redox capacity and works in a narrow potential window, whereas the second electrode utilizes large potential window and stores charges mainly in the electrical double layer (EDL). One of the first hybrid cells proposed by Razumov et al., utilized activated carbon as an EDL negative electrode and nickel hydroxide as positive electrode material in aqueous potassium hydroxide electrolyte [25]. Later, a hybrid cell was realized with H_2SO_4 electrolyte, $PbO_2/PbSO_4$ as the positive battery-like electrode, and activated carbon as negative electrode [23]. These hybrid cells displayed capaci-

* Corresponding author.
E-mail address: qamar.abbas@tugraz.at (Q. Abbas)

https://doi.org/10.1016/j.electacta.2020.135785
0013-4686/

tances twice that of their symmetric counterparts with carbon electrodes and voltages in the range of 1.5–1.7 V.

The main advantage of a hybrid cell is its high capacitance caused by the high capacity of the redox electrode, which is compensated by the high amount of charge stored on the EDL electrode according to the following equations:

$$q_+ = q_- \quad (1)$$

$$C_+ \times \Delta E_+ \times m_+ = C_- \times \Delta E_- \times m_- \quad (2)$$

where q_+ and q_- are the capacities of positive and negative electrodes, m_+ *and* m_- their active masses, while C, ΔE are the specific capacitance and potential window of electrodes, respectively.

In recently proposed hybrid cells, redox active species introduced into the aqueous electrolyte undergo faradaic reactions on one of the carbon electrodes making it battery-like, while the second carbon electrode stores charge in the EDL. According to Akinwolemiwa et al., such faradaic reactions follow Nernstian behavior owing to charge transfer involving localized electrons at a specifically fixed energy level [26]. Redox active species such as bromide [27], iodide [28], hexacyanoferrate [29,30], thiocyanide [31], vanadium complexes [32,33], and many others [34–37] have been used with aqueous electrolytes in order to enhance the cell capacitance resulting in improved energy performance.

Hybrid cells using hydroquinone as redox specie in aqueous H_2SO_4 as supporting electrolyte exhibited nearly twice the capacitance of their symmetric counterparts with e.g., chemically activated carbon, carbon aerogel, multiwalled carbon nanotubes as electrode materials [38]. A carbon/carbon hybrid cell using H_2SO_4/hydroquinone as redox active aqueous electrolyte demonstrated ~120 F g^{-1} compared to 72 F g^{-1} for the symmetric cell using neat aqueous H_2SO_4 electrolyte. However, the main drawback with this hybrid cell is the high rate of self-discharge due to the shuttling of quinone species between the two electrodes [39]. In order to reduce the high self-discharge rate, an ion exchange membrane was used as separator to limit the transfer of quinones to the negative electrode, however, with minuscule improvement [40]. Grafting of anthraquinones on the surface of carbon reduces the self-discharge behavior of hybrid cells. In this case, a cell with H_2SO_4 electrolyte, grafted carbon as negative electrode and a non-grafted carbon as positive electrode discharges to half of the initial voltage in 6 h (still far below the industrially required standard), compared to only 0.6 h discharge time for a carbon/carbon cell using H_2SO_4/HQ electrolyte [41]. Bromides and thiocyanates are also interesting redox active species for hybrid cells with aqueous electrolytes, however, the redox potential of both these couples is far away from the cell equilibrium potential (potential at discharged state, E_{0V}). This causes performance degradation due to the fact that the cell needs to be polarized to higher voltages for reaching the redox potentials. A performance comparison of iodides versus bromides based dissolved redox species in carbon/carbon cell is reported in Ref. [26] where current peaks at low cell voltage appear for iodides, contrary to bromides for which equilibrium potential is far from potential of $Br^-/Br_2 + Br_3^-$ redox reaction.

From the foregoing, it is clear that a hybrid cell exhibits improved performance when i) active species are immobilized on the redox electrode surface and ii) the redox potential of active species is close to the cell equlibrium potential. Iodide redox species fulfill the above criteria, while being highly soluble in aqueous electrolyte [28]. Moreover, iodide electrolytes based carbon/carbon cells are probably the best example of hybrid electrochemical capacitors (in aqueous electrolyte) which originates from coupling of two different charging mechanisms at both electrodes. As the redox electrode works in a small potential window, the negative electrode charges by EDL and works in large potential window. The outcome of the hybrid capacitor is a linear charge/discharge curve (similar to its negative EDL electrode or any other EDLC), from which capacitance values can be calculated after estimating the amount of energy under discharge curve. A similar charging behavior of two electrode exists in lithium-ion capacitors where the term capacitance (in F g^{-1}) is frequently used at industrial level and it is quite reasonable for good performance comparison across various capacitor devices. For the hybrid cell with aqueous Li_2SO_4/KI electrolyte, energy performance can approach to that of an EDLC with organic electrolytes [42,43]. Also, the immobilization of iodides in the positive porous carbon electrode prevents it from oxidation by keeping the potential almost constant and far below the thermodynamic oxidation potential of water [44]. Thanks to the immobilization of iodides in the porous carbon electrode associated with extensive charge transfer [45], the potential profile of the positive electrode, which is very close to cell equilibrium potential, remains nearly constant and decays only slightly during an open circuit voltage test [46]. The following reactions (equations (3)–(7)) have been proposed to occur at the positive carbon electrode with the iodide/iodine redox couple forming oligomeric iodides:

$$2I^- \leftrightarrow I_2 + 2e^- \quad (3)$$

$$I^- + I_2 \leftrightarrow I_3^- \quad (4)$$

$$I_3^- + I_2 \leftrightarrow I_5^- \quad (5)$$

$$2I_3^- \leftrightarrow 3I_2 + 2e^- \quad (6)$$

$$I_2 + 6H_2O \leftrightarrow 2IO_3^- + 12H^+ + 10e^- \quad (7)$$

Among these, reaction (7) takes place at high positive potentials ~ 0.8 V vs SHE, according to the Pourbaix diagram [47]. Despite the strong immobilization of polyiodides inside the pores of the positive carbon electrode, some of these polyiodides are transported via shuttling to the negative electrode, which results in relatively high self-discharge rates and performance degradation and in some cases, the negative electrode may even partially operate in the redox potential region of the iodides, adding to the performance loss of the hybrid cell [48]. Equally important, the electrode mass changes associated with polyiodide immobilization may alter the operating potential range of both positive and negative electrodes (see equation (2)). The effects of electrode mass-balancing have been investigated previously in the case of a carbon/CNT + polyaniline hybrid cell, a carbon/MnO_2 asymmetric device [49,50], and in carbon/carbon cells [51]. In order to balance the capacity generated by the reactions on the redox electrode, the mass ratio of the electrodes must be carefully adjusted. This becomes even more important in the case of iodides, which progressively immobilize inside the pore of the positive electrode during each voltage step leading to an enhanced mass of the redox electrode and consequently shifting the equilibrium potential.

In this work, we report on how the change in electrode mass ratio affects the equlibrium potential in a hybrid cell with aqueous iodide electrolyte. For a carbon/carbon hybrid cell with aqueous $NaNO_3$/NaI electrolyte, the progressive mass increase of positive electrode due to the immobilization of polyiodide species shifts the cell equilibrium potential. An appropriate mass-balancing of electrodes is therefore necessary which would allow the battery-like positive electrode to strictly operate at the redox potential of iodide, close to the equilibrium potential of the cell. Shift of equilibrium potential also influences the charge transfer between electrode carbon material and iodine/iodides. Overall, any shift of equilibrium potential affects the performance of hybrid cell which performance can range from a true hybrid capacitor (redox and EDL charging well-separated at the positive and negative electrode respectively) to a hybrid device with mixed EDL and faradaic charge storage at the positive electrode.

2. Experimental

2.1. Electrode and electrolyte materials

Discs of activated carbon cloth (ACC) 507–20 from Kynol were used as freestanding positive electrodes with three different mass ratios to the negative electrode (1:2, 1:1, and 2:1). The thickness of the positive electrode in all cases was 200 μm and for balancing the mass, the diameter of the disks was adjusted accordingly. The negative electrode was a KOH-activated carbon (MSP-20, from Kansai Coke and Chemicals, Japan). The porous structure of both carbons used in this study is described in ref. 45. The freestanding negative electrodes were prepared from MSP-20, 90 wt % carbon powder by mixing with 5 wt% carbon black (C65 from Imerys) as conductivity additive and 5 wt% of PTFE (60% dispersion in water from 3 M Chemicals) in ethanol. The mixture was continuously stirred at 70 °C until the solvent had completely evaporated and a dough was obtained, which was then pressed and rolled on a glass plate into a sheet. Disc electrodes were punched out from the sheet and dried at 120 °C resulting in a final thickness of 150 μm. The mass of the negative electrode was 7.5 mg while the mass of the positive electrode was varied according to the electrodes mass ratio given above. Sodium iodide (NaI, 99.5%) and sodium nitrate ($NaNO_3$, 99.8%) were purchased from Alfa-Aeser and dried at 110 °C overnight before preparing the aqueous electrolyte of 5 mol L^{-1} $NaNO_3$ + 0.5 mol L^{-1} NaI in de-ionized water. The pH of the electrolyte was 6.5 and the conductivity 92 mS cm^{-1}.

2.2. Assembling and electrochemical characterization of hybrid cells

Electrochemical investigations were performed in two-electrode cells made from PTFE Swagelok-type vessels with and without reference electrodes. Stainless steel cylinders (1.4571/1.4404) of 1.2 cm diameter were used as current collectors for the disks of working and counter electrode. A glassy microfiber separator (Whatman GF/A, thickness 260 μm) soaked in 5 mol L^{-1} $NaNO_3$ + 0.5 mol L^{-1} NaI electrolyte, which had been degassed for 15 min under reduced pressure at 24 °C was sandwiched between the disc electrodes. A silver/silver chloride (Ag/AgCl in KCl_{sat}, E = +0.197 V vs. standard hydrogen electrode [SHE]) reference electrode (from ProSense) was used to monitor the potential of the positive and negative electrodes. Hybrid cells of various electrode mass ratios in 5 mol L^{-1} $NaNO_3$ + 0.5 mol L^{-1} NaI were assembled with ACC positive electrodes of varying masses and MSP-20 as negative electrodes. These hybrid cells were tested at each voltage step with the following electrochemical protocol. Cyclic voltammetry (ν = 2 mV s^{-1}) and galvanostatic cycling at 0.1 A g^{-1} and 0.5 A g^{-1} with potential limits (GCPL) between U = 0.1 V and U = 1.5 V. Afterwards, 100 galvanostatic charge/discharge cycles using 0.5 A g^{-1} were performed up to U = 1.5 V for optimal conditioning and for monitoring any equilibrium potential shift. For two-electrode cell investigations, cyclic voltammograms (CVs, ν = 5 mV s^{-1}) and galvanostatic charge/discharge curves (0.5 A g^{-1}) before and after 100 cycles were compared. In order to avoid the intermixing of potential windows of battery-like and capacitor electrodes, the hybrid cells were discharged down to 0.1 V, which gave a buffer of ~50 mV for each electrode upon discharge to equilibrium potential (in this case $E_{0.1V}$). Precisely, this protocol prevents the undesired iodide redox reaction on the negative electrode occurring near E_{0V}, which in principle should store charges only at the EDL for a true hybrid capacitor. The long term performance of hybrid capacitor with electrode mass ratio 1:2 was evaluated during 5000 galvanostatic charge/discharge cycles at 0.5 A g^{-1}. A VMP3 multichannel potentiostat/galvanostat (Bio-Logic Instruments) was used for all electrochemical measurements. The gravimetric capacitance C was calculated by integrating the area under the galvanostatic discharge curve and expressed per total active mass of the two electrodes in F g^{-1}. The energy efficiency was estimated by the ratio of the integrated area under the galvanostatic discharge and charge curves.

2.3. Investigations on pre-polarized electrodes by thermogravimetry and Raman spectroscopy

Post-mortem analysis on the electrodes was performed by carefully disassembling the hybrid cells and taking out the positive electrodes for thermogravimetry (TGA) or Raman spectroscopy. For TGA, the polarized positive battery-like electrodes were extracted from each hybrid cell, cleaned with water, dried at 80 °C for 10 h and then hermetically sealed in aluminum crucibles. Thermogravimetric analysis was performed on a STA 449C Jupitar from Netzsch under helium flow in the temperature range of 100 °C–550 °C at a heating rate of 10 °C min^{-1}. Raman spectra were measured on freshly polarized ACC positive battery-like electrodes extracted from the hybrid cells. The positive electrodes were transferred immediately after disassembling the hybrid cell to a Horiba Jobin Yvon LabRam 800 HR spectrometer equipped with a 1024 × 256 CCD (Peltier-cooled) and an Olympus BX41 microscope. A laser wavelength of 633 nm was used for all measurements. The carbon electrode's surface was characterized by scanning electron microscope Zeiss Sigma 300 VP with a fully integrated EDS Detector Oxford SDD 80 possessing a special feature of large area mapping for detecting elemental distribution.

3. Results and discussion

Three different hybrid electrochemical cells with 5 mol L^{-1} $NaNO_3$ + 0.5 mol L^{-1} NaI have been studied, where the positive to negative electrode mass ratio was gradually increased. The effect of varying the electrode mass ratio on the equilibrium potential and the overall electrochemical performance of the hybrid cells was monitored. Following sections detail the electrochemical and physicochemical investigation on hybrid cells and electrodes with different mass ratio.

3.1. The electrode mass ratio of 1:2 for (+)ACC/MSP-20(−) in the hybrid cell

Fig. 1a shows the cyclic voltammograms obtained in a three-electrode cell equipped with reference electrode before and after 100 cycles. It can be seen that both CVs are almost identical. The unchanged electrochemical characteristics for this hybrid cell are also confirmed by the potential evolution of each electrode during the CV. The positive electrode operates in a narrow potential window due to the iodide redox reactions, which impart the high capacity. In order to compensate for the high positive electrode capacity, the negative electrode utilizes a large potential range, storing the charge in the electrical double layer (EDL). Galvanostatic charge/discharge curves at 0.1 A g^{-1} in Fig. 1b also show a narrow potential range of positive electrode (from 0.33 V to 0.56 V vs SHE) and an enlarged potential range for the negative electrode (from 0.21 V to −0.93 V vs SHE) with nearly symmetric shape of the curves after 100 cycles. Similar charging/discharging behavior of the positive battery-like electrode operating in narrow potential window was observed by Akinwolemiwa et al. [26], where oxidation of iodide was observed at low cell voltage close to the equilibrium potential (potential of zero charge, E_{0V}). The symmetric part of the charge/discharge curve of the negative electrode shows the charge storage essentially in the EDL, whereas the positive electrode displays a typical battery-like behavior with a high capacity of ~65 mAh g^{-1}. The negligible plateau of the negative electrode potential profile at the most negative values indicates the onset of other faradaic processes related to the electrochemical reduction of water [19].

The galvanostatic charge/discharge curves for the negative electrode in Fig. 1c obtained at a high specific current of 0.5 A g^{-1} are truly symmetric, which indicates that charges storage takes place in

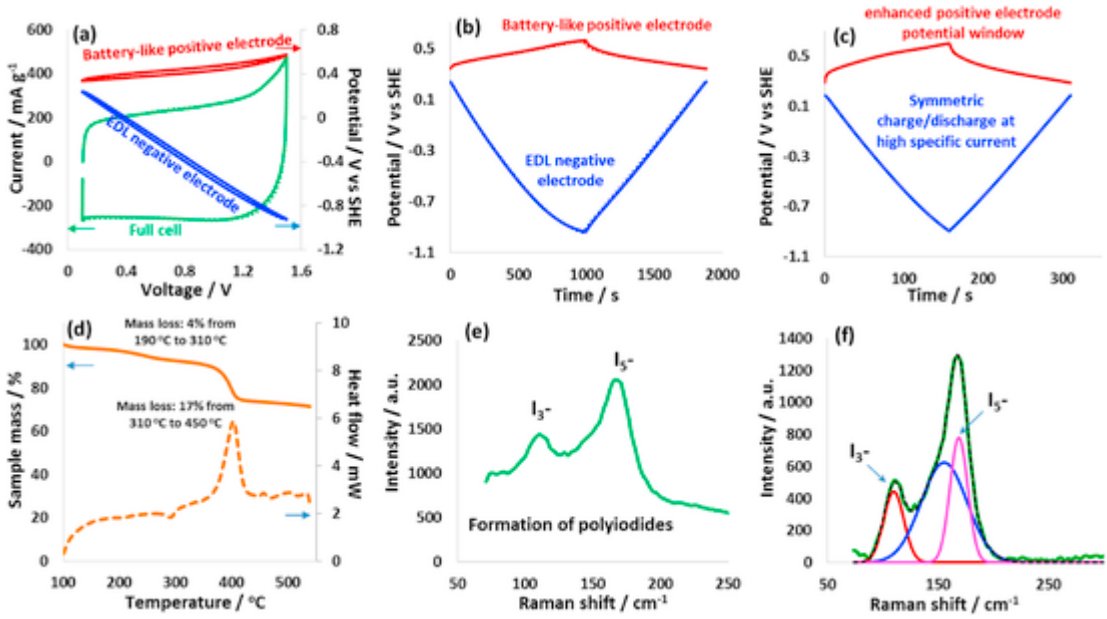

Fig. 1. Electrochemical data from two-electrode cell with reference electrode with positive (ACC) to negative electrode (MSP-20) mass ratio of 1:2 in 5 mol L^{-1} $NaNO_3$ + 0.5 mol L^{-1} NaI, (a) cyclic voltammogram at ν = 2 mV s^{-1}, (b) galvanostatic charge/discharge at 0.1 A g^{-1} (c) galvanostatic charge/discharge curve at 0.5 A g^{-1}; physicochemical analysis of the positive ACC electrode extracted from a hybrid cell after 100 galvanostatic charge/discharge cycles at 0.5 A g^{-1}, (d) thermogravimetric analysis TG & DTA curves from 100 °C to 550 °C, (e) Raman spectrum from 50 cm^{-1} to 250 cm^{-1} showing the presence of I_3^- and I_5^-, (f) deconvoluted Raman spectrum in the polyiodide region showing the subpeaks. Solid and dashed lines in Fig. 1a and b indicate the curves before and after 100 cycles.

the EDL and a positive shift of the equilibrium potential. The potential of the positive electrode is slightly pushed more positive. Upon increasing the specific current, the negative electrode works in a potential range from 0.19 V to −0.88 V vs SHE, which is slightly more positive than that at low specific current and therefore less susceptible to faradaic reactions, i.e. hydrogen evolution due to the electrochemical reduction of water. On the other hand, the positive electrode operates in a potential range from 0.29 V to 0.60 V vs SHE. The maximum potential of the positive electrode is shifted slightly towards more positive values, albeit far below the thermodynamic potential of electrolye oxidation. The positive electrode nevertheless keeps a high capacity of 56 mA h g^{-1} due to the iodide redox acitivity, when a high specific current of 0.5 A g^{-1} is applied.

Under polarization, the iodide species are adsorbed on the positive electrode blocking partly its pores, as previously reported [44]. From the TG and DTA curves in Fig. 1d, mass loss is observed in two different temperature ranges. The first mass loss of 4.1% at 190 °C–310 °C is due to the decomposition of iodides adsorbed on the electrode surface and immobilized inside the macro- and mesopores. The second mass loss of 17% occurs from 310 °C to 450 °C, which is due to the decomposition of iodine trapped in the micropores of the positive carbon electrode. This is also confirmed by the strong peak in the DTA curve at ~400 °C indicating the presence of large amounts of iodine at the positive electrode. Iodine is formed inside the pores of the positive electrode via the redox reaction in equation (1). In the next step, molecular iodine combines with iodide ions present in the bulk electrolyte to form polyiodides (I_3^- and I_5^-). The nature of these polyiodides has been cofirmed by Raman spectroscopy (Fig. 1e) of the freshly polarized positive electrode in the low wavenumber region, where two distinct bands related to the presence of I_3^- and I_5^- can be observed. The relative intensity of these two bands is different, which indicates that I_5^- is the dominant specie at the positive redox electrode. It can also be inferred that I_3^- is further converted to I_5^-, when more molecular iodine is produced (equation (3)). According to the Pourbaix diagram, at neutral electrolyte pH, the iodide ions are converted to triiodides owing to the formation of molecular iodine as given in equation (4). Further analysis in the low wavenumber region of the Raman spectrum by peak deconvolution is presented in Fig. 1f. The position of the first peak related to triiodide [ν_s (I_3^-)] remains nearly unchanged at 110 cm^{-1}, whereas the larger second peak is deconvoluted into two sub-peaks, one at 147 cm^{-1} and the other at 166 cm^{-1}, which is well known for V-shaped pentaiodide (I_5^-) [52–59]. Several possibilities exist for the sub-peak at 147 cm^{-1} which may be due to either linear I_5^- [58], L-shaped I_5^- [57] or an I_2:I_3^- adduct [57]. In the literature, this vibration at 147 cm^{-1} has also been assigned to the ν_3 antisymmetrical stretching mode of discrete asymmetric triiodide ions [60]. Overall, the formation of I_5^- and I_3^- is favored when the positive electrode is working strictly in the redox potential range of iodine. Thanks to the low mass ratio of the positive electrode and consequently a high capacity, its potential range is perfectly placed in the potential region of the iodide/iodine redox couple and the equilibrium potential remains almost unchanged during 100 galvanostatic charge/discharge cycles. The reversible formation of polyiodides is thermodynamically favored in this potential range via the formation of molecular iodine or other related species at this carbon electrode mass ratio in 5 mol L^{-1} $NaNO_3$ + 0.5 mol L^{-1} NaI. In the next sections, the influence of increasing the mass of the positive electrode on the potential range of the electrodes, the cell equilibrium potential and the overall electrochemical behavior of these hybrid cells will be discussed.

3.2. The electrode mass ratio of 1:1 for (+)ACC/MSP-20(−) hybrid cell

If the mass of the positive electrode is increased compared to the case discussed in section 3.1, the equilibrium potential shifts negatively, as depicted in the cyclic voltammograms in Fig. 2a before and after 100 galvanostatic cyles. The two-electrode cyclic voltammogram after 100 cycles is deformed at low voltage and the shift of the electrode potentials is also indicated by the deviation of the potential profiles in the low potential regions. Such a shift of equilibrium potential is driven by the asymmetric charging behavior of the electrodes (developed *in situ* due to progressive iodide immobilization) in this hybrid cell and consequently, the negative electrode is driven to too low negative potentials. The CVs in Fig. 2a show an increased current at the terminal voltage of 1.5 V and the galvanostatic charge/discharge

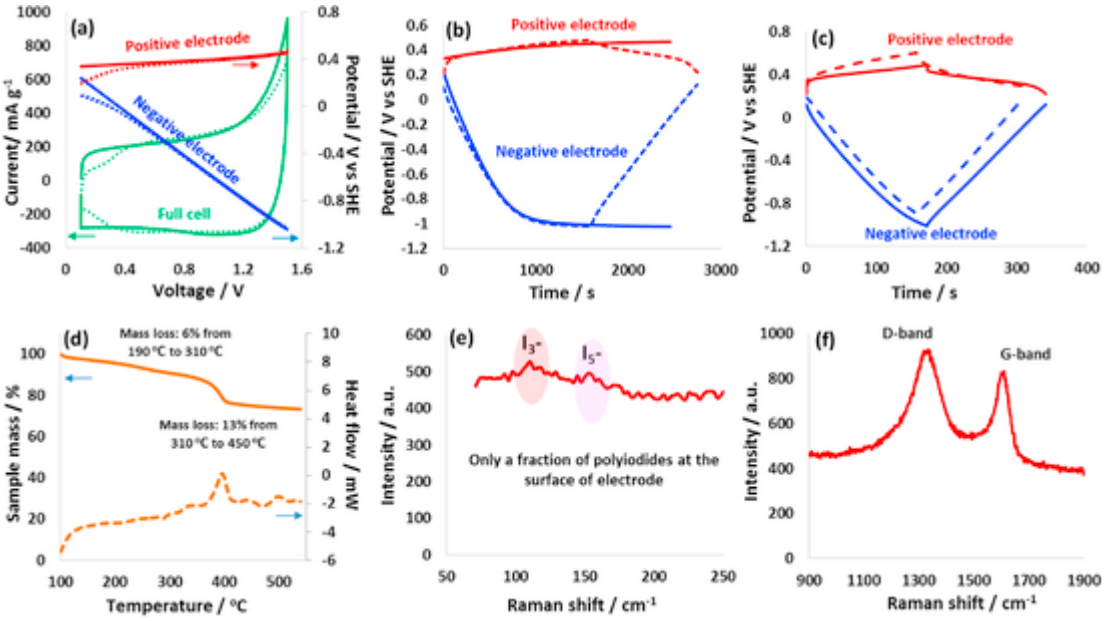

Fig. 2. Electrochemical data from two-electrode cell with reference electrode where positive (ACC) to negative electrode (MSP-20) mass ratio of 1:1 was used in 5 mol L^{-1} $NaNO_3$ + 0.5 mol L^{-1} NaI, (a) cyclic voltammogram at 2 mV s^{-1}, (b) galvanostatic charge/discharge at 0.1 A g^{-1} (c) galvanostatic charge/discharge curve at 0.5 A g^{-1}; physicochemical analysis of the positive ACC electrode extracted from a hybrid cell after 100 galvanostatic charge/discharge cycles at 0.5 A g^{-1}, (d) thermogravimetric analysis TG & DTA curves from 100 °C to 550 °C, (e) Raman spectrum of positive ACC electrode from 50 cm^{-1} to 250 cm^{-1} showing the presence of I_3^- and I_5^-, (f) D- and G-bands of Raman spectrum on positive electrode. Solid and dashed lines in Fig. 1a–c indicated the curves before and after 100 cycles.

curve (Fig. 2b) is not able to reach to the designated voltage of 1.5 V during the first cycle (solid line). Such an electrochemical response is attributed to the negative electrode working at low negative potentials where reduction reactions of water are hindered by the presence of iodide species [45], marked by the plateau of potential profile. However, after some cycles and the resulting shift in the equilibrium potential, the hybrid cell is able to reach the voltage of 1.5 V (Fig. 2b). At 1.5 V, the positive electrode operates in potential window of 0.26 V vs SHE to 0.48 V vs SHE and the negative electrode from 0.07 V vs SHE down to −1.01 V vs SHE. Nevertheless, the presence of a plateau in the negative electrode potential profile suggests the strong influence of iodide on the faradaic processes related to the electrochemical reduction of water at neutral pH and the overpotential at negative electrode.

When the specific current is increased as shown in Fig. 2c, the negative electrode exhibits symmetric charge/discharge curves, because faradaic reactions have less influence at high specific currents. Nevertheless, the cell loses capacitance after a few cycles, which is indicated by the short discharge time. The positive electrode displays mixed behavior both capacitive EDL charging and faradaic reactions due to the negative shift of the equilibrium potential. Consequently, at high specific current, the positive battery-like electrode operates in a wide potential range of 0.19 V–0.59 V vs SHE, which is about 70 mV larger than that described in section 3.1, contributing to enhanced EDL charging of the hybrid cell at low voltage.

The thermogravimetry curve in Fig. 2d shows that the decomposition of iodide species takes place in two steps similar to the case presented in section 3.1. However, the first mass loss from 190 °C to 310 °C is slightly higher in Fig. 2d with 6% compared to 4.1% in Fig. 1d. The second mass loss in Fig. 2d from 310 °C to 450 °C is 13%, which is slightly lower than in Fig. 1d, indicating that more of the iodide species are weakly adsorbed on the surface of the electrode and thus easily desorbed. On the other hand, the formation of iodine is less favored in the case of equal masses of both electrodes due to the mixed EDL and faradaic charge storage mechanisms on the same electrode. It is likely that the polyiodides, which are formed at the positive electrode, are immobilized deep in the carbon pores and therefore not easily desorbable. The low intensity of the bands for I_3^- and I_5^- in the Raman spectrum of Fig. 2e confirms their absence on the outer electrode surface. Nevertheless, polyiodides still affect the position of the D- and G-bands of the carbon (Fig. 2f), which will be discussed in section 3.4. This indicates a certain degree of charge transfer between the carbon host and polyiodides causing also changes in carbon lattice.

3.3. The electrode mass ratio of 2:1 for (+)ACC/MSP-20(−) hybrid cell

Increasing the positive over negative electrode mass ratio to 2:1 for the hybrid cell in aqueous 5 mol L^{-1} $NaNO_3$ + 0.5 mol L^{-1} NaI shifts the equilibrium potential to even more negative values. Now the redox potential range of the iodide species at the positive electrode is very narrow, as shown in Fig. 3a. The positive electrode in this hybrid cell clearly demonstrates charge storage by combined EDL and Faradaic processes. The EDL charge storage takes place close to the equilibrium potential in the region between 0.01 V and 0.25 V vs SHE and the redox active region is from 0.25 V to 0.50 V vs SHE. Given that the total potential window of the positive electrode is nearly equally shared between the charging processes of the EDL and the iodide redox activity and that the equilibrium potential is close to 0 V vs SHE, the negative electrode is pushed to work at very negative potentials. At a cell voltage of 1.5 V, the negative electrode exhibits a charging plateau at about −1.0 V vs SHE, which is due to the electrochemical reduction of water as discussed already for the previous case in section 3.2. Upon increasing the specific current (Fig. 3b), the charge/discharge curve of the negative electrode is more symmetric (fast charging shifts the equilibrium potential to slightly positive values) and the potential of the positive electrode ranges from 0.11 V to 0.33 V vs SHE for the EDL part and from 0.33 V to 0.52 V vs SHE for the iodide redox region. Hence, the positive electrode keeps the mixed EDL/redox charging characteristics at high specific current. Nevertheless, the potential of the positive electrode remains far below the thermodynamic oxidation potential of the electrolyte, preventing oxidation of the carbon material. Overall, the galvanostatic charge/discharge curve of the hybrid cell consists of two regions, which evolve under the influence of the positive electrode: i) the initial charging region at low voltage follows the EDL part

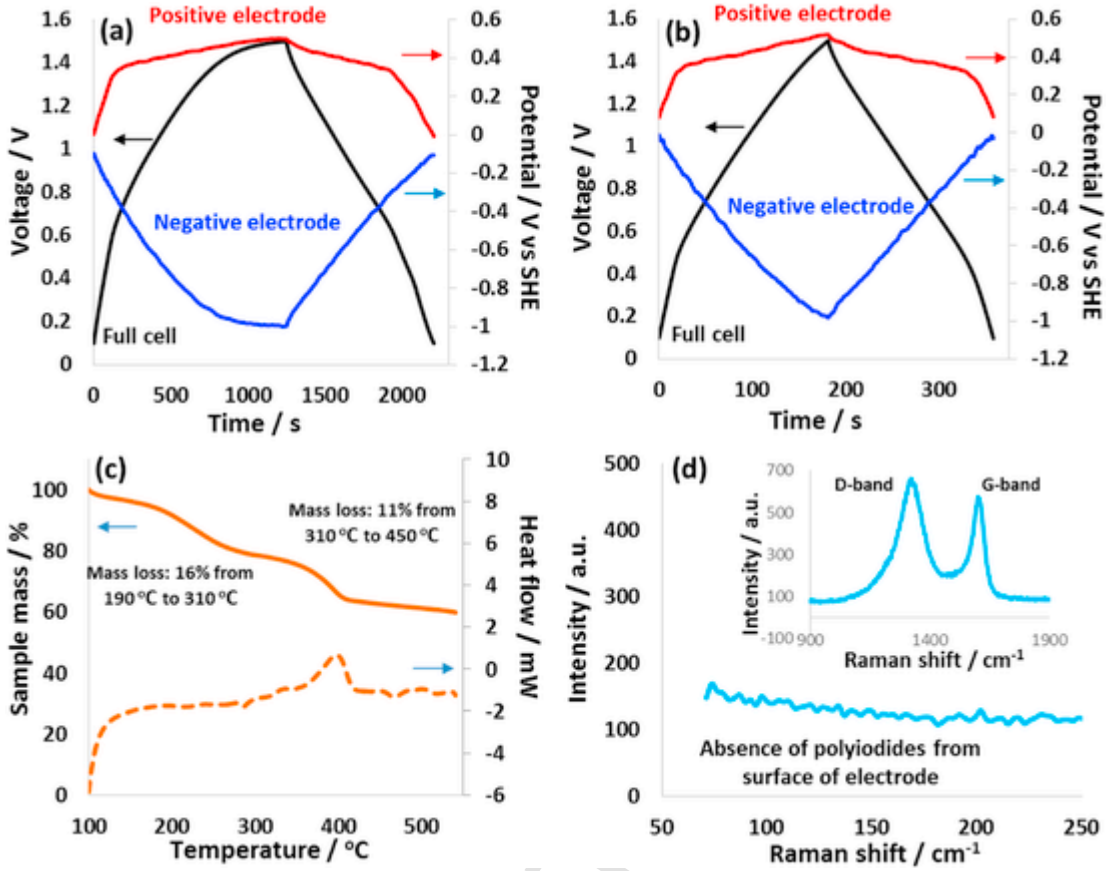

Fig. 3. Two-electrode hybrid cell equipped with a reference electrode with positive (ACC) to negative electrode (MSP-20) mass ratio of 2:1 in 5 mol L^{-1} $NaNO_3$ + 0.5 mol L^{-1} NaI, (a) galvanostatic charge/discharge at 0.1 A g^{-1} (b) galvanostatic charge/discharge curve at 0.5 A g^{-1}; physicochemical analysis of the positive ACC electrode extracted from a hybrid cell after 100 galvanostatic charge/discharge cycles at 0.5 A g^{-1}, (c) TG & DTA curves from 100 °C to 550 °C, (d) Raman spectrum from 50 cm^{-1} to 250 cm^{-1} for polyiodide region and inset showing D- and G-bands for the carbon.

of charge/discharge of the positive electrode, and ii) the high voltage region, which demonstrates high capacitance owing to the strong redox contribution of the positive electrode, while the negative electrode stores charges essentially in the EDL. With increased mass ratio of positive over negative electrode (2:1), clearly mixed behavior of typical EDL and redox charge/discharge can be seen for a hybrid cell.

The thermogravimetric analysis in Fig. 3c demonstrates two distinct mass loss regions. The first from 190 °C to 310 °C consisting of 16% and the second from 310 °C to 450 °C with 11% mass loss of the electrode. A high mass loss at relatively low temperatures and the absence of polyiodides in the Raman spectrum presented in Fig. 3d are in sharp contrast to the cases presented in sections 3.1 and 3.2. Due to the mixed charging behavior of the positive electrode, it operates only briefly in the iodide potential region. Therefore, less iodide is oxidized to iodine consequently forming smaller amounts of polyiodides. The latter are probably trapped deep inside the pores and not present at the electrode surface. The first high mass loss in the TGA curves suggests that firstly, the adsorbed iodides are accumulated on the outer surface and secondly, the polyiodides are produced in low amounts due to less available iodine in the pores. Moreover, these polyiodides are immobilized deeply in the pores of the electrode, which is confirmed by the TGA analysis and the fact they are not detectable by Raman spectroscopy. Overall, Fig. S1 summarizes a comparison between thermogravimetric (TG, DTA) and Raman analysis (iodide, D- and G-band) of three positive ACC electrodes from sections 3.1 to 3.3.

3.4. Equilibrium potential and the charge transfer at electrified carbon/iodide interface

The potential range harnessed by the positive ACC electrode in a hybrid cell with 5 mol L^{-1} $NaNO_3$ + 0.5 mol L^{-1} NaI is dependent on the equilibrium potential which in turn is strongly shifted by varying the mass ratio of the two electrodes. The extent of interaction of the polyiodides with the positive carbon electrode and related structural changes are indicated by the disorder induced D-band and the first-order graphitic G-bands in the Raman spectra in Fig. 4 for the previously discussed three cases . The low wavenumber region related to I_3^- and I_5^- detection is presented in the inset (a) and the magnified D and G-bands in insets (b) and (c) respectively. The polyiodides are more clearly visible in case of electrode mass ratio 1:2 while there is gradual decrease of signals with increasing positive electrode mass ratio. It appears that as soon as the positive electrode demonstrates mixed EDL and battery-like charge/discharge character, the polyiodides formation is probably less favored due to lack of molecular iodine (equations (3)–(5)). The interaction of polyiodides with the positive carbon electrode has been described as a charge transfer [61]. Upon the interaction with iodine/polyiodides, the lattice of carbon material undergoes structural changes which are indicated by the shifts of D- and G-bands.

Compared to the pristine ACC electrode, an upshift of both the bands has been observed for the positive electrode in these hybrid cells. It can be also seen that the G-band demonstrates lesser upshift in all three cases as compared to the D-band. An upshift of ca. ~3 cm^{-1} for the G-band (in all three cases in the present study) is in similar range to the previously reported one where hybrid cell used 1 mol L^{-1}

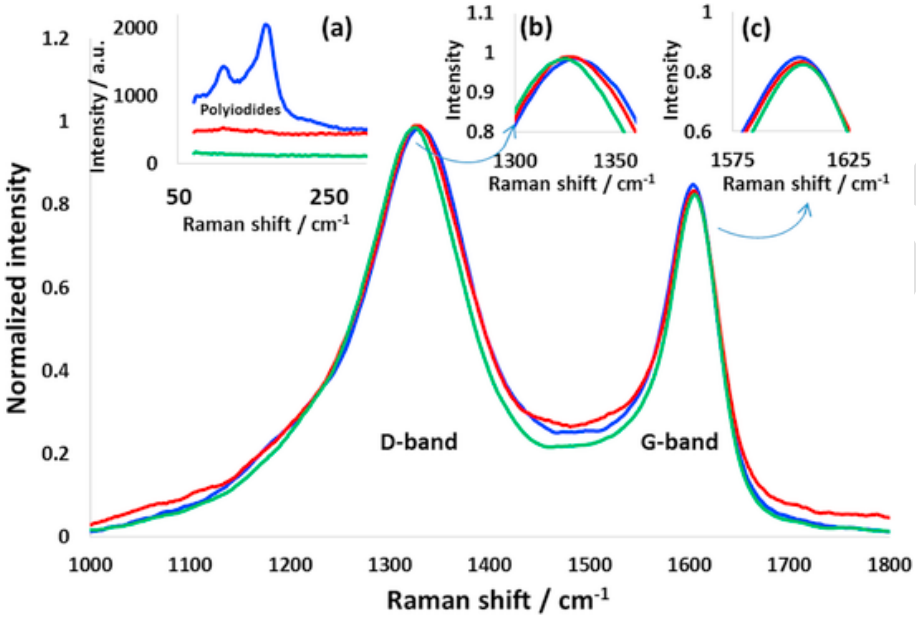

Fig. 4. Raman spectra of positive ACC electrodes extracted from hybrid cells (after 100 galvanostatic charge/discharge cycles at 0.5 A g^{-1}) in 5 mol L^{-1} $NaNO_3$ + 0.5 mol L^{-1} NaI with positive to negative electrode mass ratio of 1:2 (blue line), 1:1 (red line) and 2:1 (green line). Inset (a) shows polyiodide region, and (b) and (c) the D- and G-bands respectively. Spectra are normalized to D-band intensity. (For interpretation of the references to colour in this figure legend, the reader is referred to the Web version of this article.)

Li_2SO_4 + 0.5 mol L^{-1} KI as electrolyte [61]. In addition, a slight enhancement in the intensity of G-band is also observed, the more the polyiodides present on the positive electrode, the higher the G-band intensity. In order to quantify the changes in Raman spectra, peaks have been deconvoluted based on a double Lorentzian for D-band and a Breit-Winger-Fano shaped for G-band [62]. The spectra are baseline corrected (linear fit) and normalized (vector normalization) for the deconvolution (see detailed deconvoluted spectra in Supplementary Information Fig. S2). Peak analysis allows for further estimating the band widths, relative band intensities and crystallite size, which have been evaluated according to the method of Tuinstra-Koenig [63] and Mallet-Ladeira et al. [64], respectively. Table 1 shows the D- and G-band upshifts and intensity ratios, as well as the width of the G-band and calculated crystallite sizes, for the positive electrodes in three hybrid cells with different electrodes mass ratio.

The D-band upshift appears to be dependent on the extent of charge transfer between positive carbon electrode and the polyiodides (I_3^- and I_5^-). The D-band is gradually upshifted and higher D-band upshift is observed for the positive electrode working strictly in the redox region of iodides and where more polyiodides are formed (hybrid cell with electrode mass ratio 1:2). Afterwards, as soon as the positive electrode demonstrates a mixed EDL and battery-like charge/discharge behavior, less D-band upshift is observed. In contrast to the D-band, the upshift of the G-band is the smallest for the electrode mass ratio of 1:2 and increases towards the 2:1 mass ratio. Further, the electrode mass ratio of 1:2 has the highest bandwidth for the G-band and the largest I_D/I_G ratio and consequently the smallest crystallite size (L_a). All of this is consistent with a slight increase of defects or decrease of crystallinity from the 2:1 to the 1:2 mass ration sample [65–68]. The G-bands behavior (upshifted relative to pristine ACC, but downshifted for the 1:2 mass sample) might be understood as a superimposition of upshift due to the charge transfer and the downshift due to the increase in defects. Nevertheless, the difference of the I_D/I_G ratio presented in Table 1 is small and might be insignificant, thus further Raman investigations on electrodes after long-term ageing are necessary. The SEM images in Fig. S3 show the areas of positive ACC electrodes (extracted from three hybrid cells) analysed by the EDS analysis and the presence of iodides on the positively polarized ACC electrodes is confirmed by these analyses. The elemental distribution in Table S1 shows that iodine is equally distributed throughout the matrix of each positive carbon electrode. However, the varying amounts of iodine from one electrode to another with changing mass ratio is a qualitative indication of the redox activity of iodide during the hybrid cell operation. Overall, the gradual shifts of D- and G-bands in Raman spectra and enhancement of mass loss during TG experiments (for hybrid cells of all mass ratio) indicate that the iodide related species are progressively adsorbed in nanoporous carbon based positive electrode. Previous investigations on carbon/iodide interface in aqueous iodide electrolytes have also shown that carbon electrode pores are eventually blocked due to the accumulation of iodine/iodide species [44,69].

Table 1
Upshifts of D- and G-bands, G-band half-width at half maximum (Γ_G), I_D/I_G ratio and L_a calculated according to Refs. [63,64] respectively for the positive electrodes extracted from hybrid cells with three different electrode mass ratios.

Electrodes mass ratio	Upshift D-band$_{positive}$ (cm^{-1})	Upshift G-band$_{positive}$ (cm^{-1})	Γ_G (cm^{-1})	I_D/I_G ratio	L_a/nm [63]	L_a/nm [64]
1:2	14.4	2.4	30.5	1.22	8.3	7.8
1:1	12.3	3.7	30.1	1.20	8.4	7.9
2:1	8.0	4.2	29.0	1.18	8.5	8.1

3.5. Performance of (+)ACC/MSP-20(−) hybrid cells in aqueous $NaNO_3$ + NaI

The hybrid cells containing three mass ratios of electrodes have been investigated between 0.1 and 1.5 V and the electrochemical data before and after 100 galvanostatic charge/discharge cycles is presented in Fig. 5. It is important to note that the cell discharge voltage was cut at 0.1 V ($E_{0.1V}$) meaning that the electrodes were prevented from discharging to the potential of zero volt. Such protocol helped to avoid the unnecessary current peak at close to 0 V as has been observed in previous studies [26] and dedicated to the iodide redox reactions on negative electrode. Thereby, effects of these redox redox reactions and re-

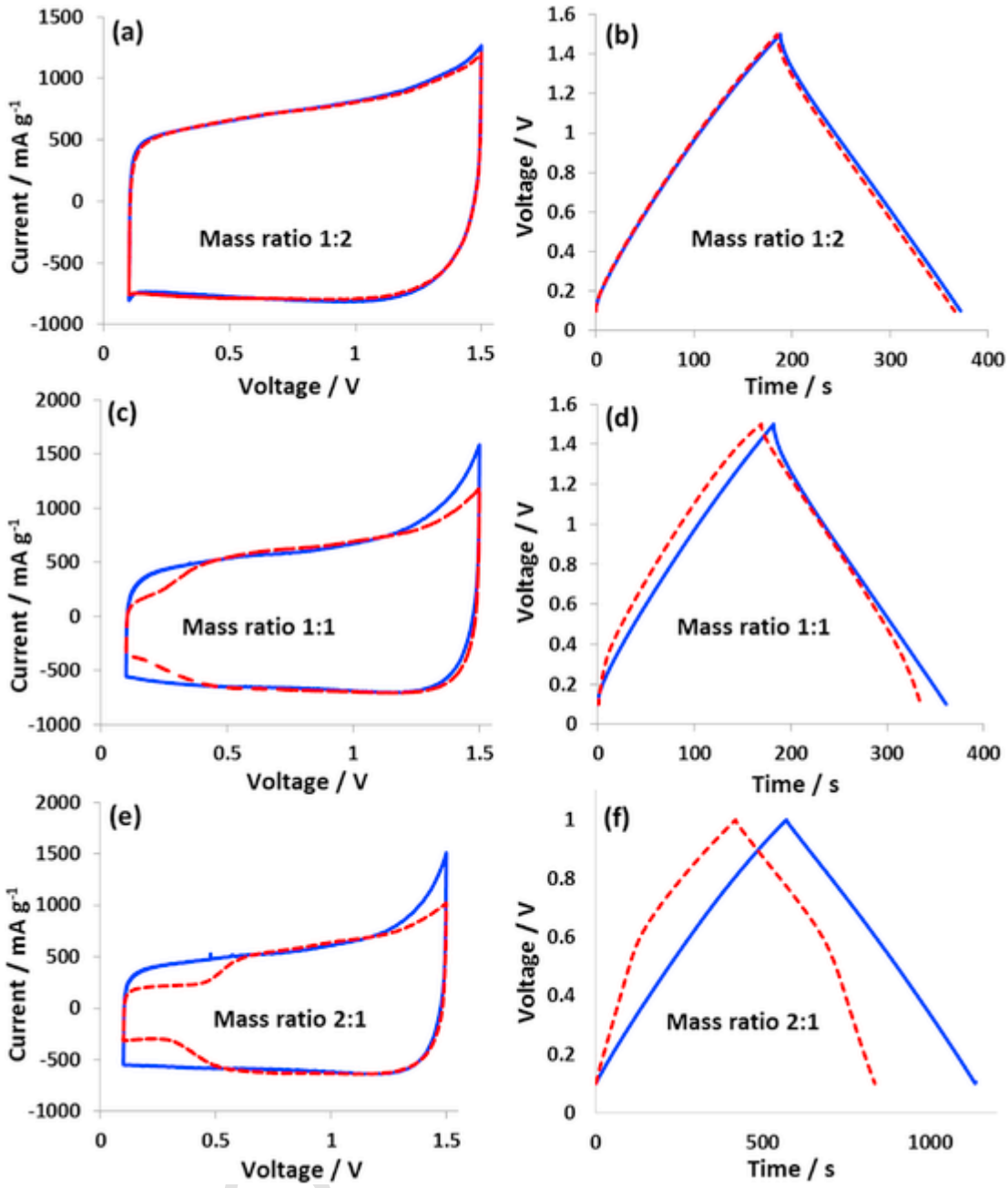

Fig. 5. Comparison of two electrode cell data before and after 100 galvanostatic charge/discharge cycles, cyclic voltammetry (a, c, e) and galvanostatic charge/discharge curves (b, d) at 0.5 A g^{-1} and (f) at 0.1 A g^{-1} for hybrid cells with mass ratios (a, b)1:2, (c, d) 1:1 and (e, f) 2:1. Full line and dashed lines indicate the curves obtained before and after the cycling period, respectively.

lated shuttling of iodides on the cyclability and overall performance were prevented for all the cells reported in this study. The energy efficiency and capacitance values are evaluated from the 100th galvanostatic charge/discharge cycle. CVs (ν = 5 mV s^{-1}) of the hybrid cell with 1:2 electrode mass ratio in Fig. 5a are rectangular before and after 100 cycles. Likewise, the charge/discharge curves in Fig. 5b maintain their symmetric profile up to 1.5 V at a specific current of 0.5 A g^{-1}. Consequently, the cell capacitance of 63 F g^{-1} at 1.0 V (which translates into 31 F cm^{-3}) and energy efficiency values remain almost constant before and after this cycling period, confirming the stable electrochemical performance of this hybrid cell with a perfect capacitor like behavior. Besides, the specific energy estimated by power tests is around 23 Wh/kg at 0.5 kW/kg. Thanks to the correct balancing of electrode capacities by adjusting the mass ratio of ACC and MSP-20 electrodes to 1:2, symmetric charge/discharge curves and square-shaped cyclic voltammograms without the current peaks near 0V were obtained (Fig. S4a,d). Anyway the influence of pore size of positive carbon electrode for accommodating and retaining the iodide species should not be ignored as discussed in Ref. [69], meaning that the electrode mass ratio might differ for $NaNO_3$ + NaI system when implementing another nanoporous electrode.

If a 1:1 electrode mass ratio is used in the hybrid cell, Fig. 5c and 5d demonstrate that the cyclic voltammograms do not keep the rectangular shape and the charge/discharge curves are no longer symmetric after 100 cycles up to 1.5 V. The resulting capacitance decreases from 60 F g^{-1} to 54 F g^{-1} at 1.0 V during cycling. The change in electrochemical behavior for a given cycling period of the hybrid cell with equal mass ratio of the two electrodes can be correlated with the

shift of equilibrium potential, as explained in section 3.2. Due to the positive electrode displaying a mixed EDL and Faradaic charge storage behavior, the electrochemical charge/discharge characteristics of the hybrid cell are modified.

Fig. 5e and 5f shows the case, where the active material mass of the positive electrode is twice that of the negative electrode. The initial cyclic voltammogram up to 1.5 V shows a high current at the terminal voltage and the initial galvanostatic charging curve up to 1.0 V is symmetric in shape. After cycling to 1.5 V, the charging characteristics are modified with a linear charging part in the initial voltage range and a plateau in the high voltage region. The capacitance decreases from 56 F g^{-1} before cycling to 41 F g^{-1} at 1.0 V. Such a behavior is a direct consequence of the shift in the equilibrium potential, which causes the positive electrode to operate with two charging mechanisms during a single scan. After 100 cycles, the energy efficiency of this hybrid cell with mass ratio 2:1 has decreased from initially 95% to 92%, confirming the previous findings of an impairing effect of the equilibrium potential shift on the cell performance. Taking into account the activated carbon density of 0.5 g cm^{-3}, the volumetric capacitance values show a similar trend as gravimetric ones and the hybrid capacitor with 1:2 mass ratio having the highest volumetric capacitance 31 F cm^{-3}, followed by 27 F cm^{-3} for 1:1 electrode mass ratio and 20 F cm^{-3} for 2:1 electrode mass ratio. Cyclic voltammograms up to 1.5 V for the two electrode hybrid cells with different electrode mass ratio after 100 cycles are also shown in Fig. S4, where a gradual shift from a hybrid capacitor to a hybrid device can be seen. Moreover, the galvanostatic charge/discharge curves are symmetric for the hybrid capacitor where electrodes are well-balanced at mass ratio 1:2. Figs. S5a and b presents the cyclic voltammograms of hybrid capacitor with electrode mass ratio 1:2 and 5 mol L^{-1} $NaNO_3$ + 0.5 mol L^{-1} NaI at various scan rates (5 mV s^{-1}, 10 mV s^{-1}, 20 mV s^{-1}, 50 mV s^{-1}, 80 mV s^{-1} and 100 mV s^{-1}) between 0.1 and 1.5 V. The hybrid capacitor keeps a high capacitance of 53 F g^{-1} at a scan rate of 50 mV s^{-1}. Fig. S5c shows a capacitance decay of ~4% after 5000 galvanostatic charge/discharge cycles at 0.5 A g^{-1} up to 1.5 V. This slight loss of capacitance could be due to the combined effect of changes at the electrode surface and iodide shuttling. As previously reported the electrochemical reduction products of nitrate such as NO, NO_2, N_2O and HNO_2 under various thermodynamic condition may contribute to oxidation of carbon electrodes surface [70–72] and related performance loss of hybrid cell. Moreover, any catalytic effect owing to the presence of nitrate ions on the conversion of iodides to iodine can not be ignored as well [73]. Overall, the electrode mass ratio of 1:2 with ACC/MSP-20 setup in $NaNO_3$/NaI proves to be the optimized one for a hybrid electrochemical capacitor with unchanged potential profiles of electrode and stable long-term cycling performance. Of course oversizing too much the negative electrode would shift the equilibrium potential to the negative values and more iodine/polyiodides would be produced at the positive electrode with risks of shuttling to negative electrode and deteriorating the hybrid cell performance.

4. Conclusion

The charge transfer at the positive carbon electrode/iodide interface in a hybrid capacitor with aqueous $NaNO_3$/NaI electrolyte is strongly influenced by changing the mass ratio of the two electrodes. This is due to the progressive increase of positive electrode mass with increasing voltage steps and the continuous adsorption of iodide inside the nanopores leading to a shift of the hybrid cell equilibrium potential and eventually to changes in the linearity of the charge/discharge curves. With an electrolyte composition of 5 mol L^{-1} $NaNO_3$ + 0.5 mol L^{-1} NaI, a positive (ACC) to negative (MSP-20) electrode mass ratio of 1:2 is found to be optimal in that the equilibrium potential shift is negligible and the hybrid cell exhibits stable performance. As the iodide/iodine immobilization is dependent on the porous nature of carbon, a different electrode mass ratio may be needed for other carbon materials to be used for building hybrid capacitor with $NaNO_3$/NaI electrolyte. Formation of iodine through iodide oxidation plays a key role in producing polyiodides. The more iodine is produced in the porosity of carbon according to equation (3), the more polyiodides are formed, which is confirmed by theromgravimetric analysis and Raman spectroscopy. The concept of electrode mass balancing has been applied to almost all energy storage systems. However, it is of utmost importance for those systems, where adsorption of species on the electrode surface is progressive, rendering the selection of the initial mass of the electrode very important. Based on these findings, a careful selection of electrodes mass ratio is recommended for hybrid cells and the mass of electrolyte should be considered as well, when reporting the capacitance and energy parameters.

CRediT authorship contribution statement

Q. Abbas: Conceptualization, Supervision, Funding acquisition, Project administration, Methodology, Writing - original draft. **H. Fitzek:** Methodology, Investigation, Writing - review & editing. **V. Pavlenko:** Methodology, Validation, Writing - review & editing. **B. Gollas:** Writing - review & editing.

Declaration of competing interest

The authors declare no conflict of interest.

Acknowledgments

Funding for this research by the Austrian Science Fund (FWF) under the Lise Meitner project M 2576-N37 is acknowledged. Q. A thanks Josefine Hobisch for assisting in carrying out the TGA related experimental work and Martin Wilkening for his continuous support.

Appendix A. Supplementary data

Supplementary data to this article can be found online at https://doi.org/10.1016/j.electacta.2020.135785.

References

[1] B.E. Conway, Transition from supercapacitor to battery behavior in electrochemical energy storage, J. Electrochem. Soc. 138 (1991) 139–1548.
[2] B.E. Conway, Electrochemical Supercapacitors: Scientific Fundamentals and Technological Applications, Kluwer Academic Plenum Publisher, New York, 1999.
[3] M. Winter, R.J. Brodd, What are batteries, fuel cells, and supercapacitors?, Chem. Rev. 104 (2004) 4245–4269.
[4] A. Burke, R&D considerations for the performance and application of electrochemical capacitors, Electrochim. Acta 53 (2007) 1083–1091.
[5] P. Simon, Y. Gogotsi, Materials for electrochemical capacitors, Nat. Mater. 7 (2008) 845–854.
[6] J.R. Miller, P. Simon, Electrochemical capacitors for energy management, Science 321 (2008) 651–652.
[7] K. Naoi, S. Ishimoto, J.I. Miyamoto, W. Naoi, Second generation nanohybrid supercapacitor: evolution of capacitive energy storage devices, Energy Environ. Sci. 5 (2012) 9363–9373.
[8] F. Béguin, V. Presser, A. Balducci, E. Frackowiak, Carbons and electrolytes for advanced supercapacitors, Adv. Mater. 26 (2014) 2219–2251.
[9] G. Wang, L. Zhang, J. Zhang, A review of electrode materials for supercapacitor, Chem. Soc. Rev. 41 (2012) 797–828.
[10] C. Zhong, Y. Deng, W. Hu, J. Qiao, L. Zhang, J. Zhang, A review of electrolyte materials and compositions for electrochemical supercapacitors, Chem. Soc. Rev. 44 (2015) 7484–7539.
[11] J.W. Long, D. Belanger, T. Brousse, W. Sugimoto, M.B. Sassin, O. Crosnier, Asymmetric electrochemical capacitors stretching the limits of aqueous electrolytes, MRS Bull. 36 (2011) 513–522.
[12] J. Chae, G. Chen, 1.9 V aqueous carbon-carbon supercapacitors with unequal electrode capacitances, Electrochim. Acta 86 (2012) 248–254.
[13] A. Bello, F. Barzegar, D. Momodu, J. Dangbegnon, F. Taghizadeh, N. Manyala, Symmetric supercapacitors based on porous 3D interconnected carbon framework, Electrochim. Acta 151 (2015) 386–392.
[14] Y. Wang, Y. Song, Y. Xia, Electrochemical capacitors: mechanism, materials, systems, characterization and applications, Chem. Soc. Rev. 45 (2016) 5925–5950.

[15] L. Xia, L. Yu, D. Hu, G. Chen, Electrolytes for electrochemical energy storage, Mater. Chem. Front. 1 (2017) 584–618.

[16] Q. Gao, L. Demarconnay, E. Raymundo-Pinero, F. Béguin, Exploring the large voltage range of carbon/carbon supercapacitors in aqueous lithium sulfate electrolyte, Energy Environ. Sci. 5 (2012) 9611–9617.

[17] S.-E. Chun, J. Whitacre, Investigating the role of electrolyte acidity on hydrogen uptake in mesoporous activated carbons, J. Power Sources 242 (2013) 137–140.

[18] Q. Abbas, P. Ratajczak, P. Babuchowska, A.L. Comte, D. Bélanger, T. Brousse, F. Béguin, Strategies to improve the performance of carbon/carbon capacitors in salt aqueous electrolytes, J. Electrochem. Soc. 162 (2015) A5148–A5157.

[19] Q. Abbas, B. Gollas, V. Presser, Reduced faradaic contributions and fast charging of nanoporous carbon electrodes in a concentrated sodium nitrate aqueous electrolyte for supercapacitors, Energy Technol. 7 (2019) 1900430.

[20] Q. Abbas, P. Ratajczak, F. Béguin, Sodium molybdate – an additive of choice for enhancing of AC/AC electrochemical capacitors in a salt aqueous electrolyte, Faraday Discuss 172 (2014) 199–214.

[21] P. Ratajczak, K. Jurewicz, P. Skowron, Q. Abbas, F. Béguin, Electrochim. Acta 130 (2014) 344–350.

[22] M. He, K. Fic, E. Frackowiak, P. Novak, E.J. Berg, Ageing phenomena in high-voltage aqueous supercapacitors investigated by in situ gas analysis, Energy Environ. Sci. 9 (2016) 623–633.

[23] W. Pell, B. Conway, Peculiarities and requirements of asymmetric capacitor devices based on combination of capacitor and battery-type electrodes, J. Power Sources 136 (2004) 334–345.

[24] B. Conway, W. Pell, Double-layer and pseudocapacitance types of electrochemical capacitors and their applications to the development of hybrid devices, J. Solid State Electrochem. 7 (2003) 637–644.

[25] S. Razumov, S. Litvinenko, A. Klementov, A. Belyakov, European Patent 1 (2001) 500 156.

[26] B. Akinwolemiwa, C. Wei, Q. Yang, L. Yu, L. Xia, D. Hu, C. Peng, G.Z. Chen, Optimal utilization of combined doubla layer and Nernstian charging of activated carbon electrodes in aqueous halide supercapattery through capacitance unequalization, J. Electrochem. Soc. 165 (2018) A4067–A4076.

[27] S. Yamazaki, T. Ito, Y. Murakumo, M. Naitou, T. Shimooka, M. Yamagata, M. Ishikawa, Hybrid capacitors utilizing halogen-based redox reactions at interface between carbon positive electrode and aqueous electrolytes, J. Power Sources 326 (2016) 580–586.

[28] G. Lota, E. Frackowiak, Striking capacitance of carbon/iodide interface, Electrochem. Commun. 11 (2009) 87–90.

[29] J. Lee, S. Choudhury, D. Weingarth, D. Kim, V. Presser, High performance hybrid energy storage with potassium ferricyanide redox electrolyte, ACS Appl. Mater. Interfaces 8 (2016) 23676–23687.

[30] K. Chen, F. Liu, D. Xue, et al., Carbon with ultrahigh capacitance when graphene paper meets $K_3[Fe(CN)_6]$, Nanoscale 7 (2015) 432–439.

[31] B. Gorska, P. Bujewska, K. Fic, Thiocyanates as attractive redox-active electrolytes for high-energy and environmentally-friendly electrochemical capacitors, Phys. Chem. Chem. Phys. 19 (2017) 7923–7935.

[32] J. Lee, B. Kruner, A. Tolosa, S. Sathyamoorthi, D. Kim, S. Choudhury, K.-H. Seo, V. Presser, Tin/vanadium redox electrolyte for battery-like energy storage capacity combined with supercapacitor-like power handling, Energy Environ. Sci. 9 (2016) 3392–3398.

[33] J. Lee, A. Tolosa, B. Krüner, N. Jäckel, S. Fleischmann, M. Zeiger, D. Kim, V. Presser, Asymmetric Tin–Vanadium redox electrolyte for hybrid energy storage with nanoporous carbon electrodes, Sustain. Energy Fuel. 1 (2017) 299–307.

[34] S.-E. Chun, B. Evanko, X. Wang, D. Vonlanthen, X. Ji, G.D. Stucky, S.W. Boettcher, Design of aqueous redox-enhanced electrochemical capacitors with high specific energies and slow self-discharge, Nat. Commun. 6 (2015) 7818.

[35] W. Chen, R.B. Rakhi, H.N. Alshareef, Capacitance enhancement of polyaniline coated curved-graphene supercapacitors in a redox-active electrolyte, Nanoscale 5 (2013) 4134–4138.

[36] S.T. Senthilkumar, R.K. Selvan, J.S. Melo, Redox additive/active electrolytes: a novel approach to enhance the performance of supercapacitors, J. Mater. Chem. A 1 (2013) 12386–12394.

[37] J. Wu, H. Yu, L. Fan, G. Luo, J. Lin, M. Huang, A simple and high-effective electrolyte mediated with p-phenylenediamine for supercapacitor, J. Mater. Chem. 22 (2012) 19025–19030.

[38] S. Roldán, C. Blanco, M. Granda, R. Menéndez, R. Santamaría, Towards a further generation of high-energy carbon-based capacitors by using redox-active electrolytes, Angew. Chem. Int. Ed. 50 (2011) 1699–1701.

[39] S. Roldan, M. Granda, R. Men, R. Santamaría, C. Blanco, Mechanisms of energy storage in carbon-based supercapacitors modified with quinoid redox-active electrolyte, J. Phys. Chem. C 115 (2011) 17606–17611.

[40] L. Chen, H. Bai, Z. Huang, L. Li, Mechanism investigation and suppression of self-discharge in active electrolyte enhanced supercapacitors, Energy Environ. Sci. 7 (2014) 1750–1759.

[41] G. Shul, D. Bélanger, Self-discharge of electrochemical capacitors based on soluble or grafted quinone, Phys. Chem. Chem. Phys. 18 (2016) 19137–19145.

[42] Q. Abbas, P. Babuchowska, E. Frackowiak, F. Béguin, Sustainable AC/AC hybrid electrochemical capacitors in aqueous electrolyte approaching the performance of organic systems, J. Power Sources 326 (2016) 652–659.

[43] P. Przygocki, Q. Abbas, B. Gorska, F. Béguin, High-energy hybrid electrochemical capacitor operating down to −40 °C with aqueous redox electrolyte based on choline salts, J. Power Sources 427 (2019) 283–292.

[44] P. Przygocki, Q. Abbas, P. Babuchowska, F. Béguin, Confinement of iodides in carbon porosity to prevent from positive electrode oxidation in high voltage aqueous hybrid electrochemical capacitors, Carbon 125 (2017) 391–400.

[45] Q. Abbas, H. Fitzek, H. Schrottner, S. Dsoke, B. Gollas, Immobilization of polyiodide redox species in porous carbon for battery-like electrodes in eco-friendly hybrid electrochemical capacitors, Nanomaterials 9 (2019) 1413.

[46] Q. Abbas, F. Béguin, Influence of the iodide/iodine redox system on the self-discharge of AC/AC electrochemical capacitors in salt aqueous electrolyte, Prog. Nat. Sci.: Mater. Int. 25 (2015) 622–630.

[47] M. Pourbaix, Atlas D'Equilibres Electrochimiques, Gauthier-Villars, Paris, 1963, p. 614.

[48] E. Frackowiak, M. Meller, J. Menzel, D. Gastol, K. Fic, Redox-active electrolyte for supercapacitor application, Faraday Discuss 172 (2014) 179–198.

[49] C. Peng, S. Zhang, X. Zhou, G. Chen, Unequalisation of electrode capacitances for enhanced energy capacity in asymmetrical supercapacitors, Energy Environ. Sci. 3 (2010) 1499–1502.

[50] V. Khomenko, E. Raymundo-Pinero, F. Béguin, Optimisation of an asymmetric manganese oxide/activated carbon capacitor working at 2 V in aqueous medium, J. Power Sources 153 (2006) 183–190.

[51] S. Vaquero, J. Palma, M. Anderson, R. Marcilla, Mass-balancing of electrodes as a strategy to widen the operating voltage window of carbon/carbon supercapacitors in neutral aqueous electrolytes, Int. J. Electrochem. Sci. 8 (2013) 10293–10307.

[52] R.C. Teitelbaum, S.L. Ruby, T.J. Marks, On the structure of starch-iodine, J. Am. Chem. Soc. 100 (1978) 3215–3217.

[53] R.C. Teitelbaum, S.L. Ruby, T.J. Marks, A resonance Raman/iodine Moessbauer investigation of the starch-iodine structure. Aqueous solution and iodine vapor preparations, J. Am. Chem. Soc. 102 (1980) 3322–3328.

[54] E.M. Nour, L.H. Chen, J. Laane, Far-infrared and Raman spectroscopic studies of polyiodides, J. Phys. Chem. 90 (1986) 2841–2846.

[55] V. Jovanovski, B. Oral, I. Jerman, S.B. Hocevar, B. Ogorevc, Electrochemical and in-situ Raman spectroelectrochemical study of 1-methyl-3-propylimidazolium iodide ionic liquid with added iodine, Electrochem. Commun. 9 (2007) 2062–2066.

[56] X. Yu, C. Houtman, R. Atalla, The complex of amylose and iodine, Carbohydr. Res. 292 (1996) 129–141.

[57] P.H. Svensson, L. Kloo, Synthesis, structure, and bonding in polyiodide and metal Iodide−Iodine systems, Chem. Rev. 103 (2003) 1649–1684.

[58] S.B. Sharp, G.I. Gellene, Ab initio calculations of the ground electronic states of polyiodide anions, J. Phys. Chem. A 101 (1997) 2192–2197.

[59] R. Kawano, M. Watanabe, Anomaly of charge transport of an iodide/tri-iodide redox couple in an ionic liquid and its importance in dye-sensitized solar cells, Chem. Commun. (2005) 2107–2109.

[60] H. Mittag, H. Stegemann, H. Füllbier, G. Irmer, Raman spectroscopic investigation of N-alkylurotropinium polyiodides, J. Raman Spectrosc. 20 (1989) 251–255.

[61] P. Przygocki, Q. Abbas, F. Beguin, Capacitance enhancement of hybrid electrochemical capacitor with asymmetric carbon electrodes configuration in neutral aqueous electrolyte, Electrochim. Acta 269 (2018) 640–648.

[62] P. Mallet-Ladeira, P. Puech, P. Weisbecker, G. Vignoles, M. Monthioux, Behavior of Raman D band for pyrocarbons with crystallite size in the 2–5 nm range, Appl. Phys. A 114 (2014) 759–763.

[63] F. Tuinstra, J. Lo Koenig, Raman spectrum of graphite, J. Chem. Phys. 53 (1970) 1126–1130.

[64] P. Mallet-Ladeira, P. Puech, C. Toulouse, M. Cazayous, N. Ratel-Ramond, P. Weisbecker, G. Vignoles, M. Monthioux, A Raman study to obtain crystallite size of carbon materials: a better alternative to the Tuinstra–Koenig law, Carbon 80 (2014) 629–639.

[65] A.C. Ferrari, J. Robertson, Resonant Raman spectroscopy of disordered, amorphous, and diamondlike carbon, Phys. Rev. B 64 (2001) 075414.

[66] M.S. Dresselhaus, A. Jorio, A. Souza Filho, R. Saito, Defect characterization in graphene and carbon nanotubes using Raman sepectroscopy, Phil. Trans. R. Soc. A 368 (2010) 5355–5377.

[67] G.D. Saraiva, A. Souza Filho, G. Braunstein, E. Barros, J. Mendes Filho, E. Moreira, S. Fagan, D. Baptista, Y. Kim, H. Muramatsu, M. Endo, M. Dresselhaus, Resonance Raman spectroscopy in Si and C ion-implanted double-wall carbon nanotubes, Phys. Rev. B 80 (2009) 155452.

[68] P. Chu, L. Li, Characterization of amorphous and nanocrystalline carbon films, Mater. Chem. Phys. 96 (2006) 253–277.

[69] J. Lee, P. Srimuk, S. Fleischmann, A. Ridder, M. Zeiger, V. Presser, Nanoconfinement of redox reactions enables rapid zinc iodide energy storage with high efficiency, J. Mater. Chem. A 5 (2017) 12520–12527.

[70] K. Fic, M. He, E.J. Berg, P. Novák, E. Frackowiak, Comparative operando study of degradation mechanisms in carbon-based electrochemical capacitors with Li_2SO_4 and $LiNO_3$ electrolytes, Carbon 120 (2017) 281–293.

[71] K. Ota, Y. Amano, M. Aikawa, M. Machida, Removal of nitrate ions from water by activated carbons (ACs) – influence of surface chemistry of ACs and coexisting chlorie and sulfate ions, Appl. Surf. Sci. 276 (2013) 838–842.

[72] L. Mei, G. Shelp, W. Chesworth, Electrochemical Treatment of Water Contaminated with Nitrogenous Compounds, European Patent, 1997 PCT/CA1997/000122.

[73] A. Boldarini Couto, S. Cassoli de Souza, E. Romão Sartori, P. Jacob, D. Klockow, E. Almeida Neves, The catalytic cycle of oxidation of iodide ion in the oxygen/nitrous acid/nitric oxide system and its potential for analytical applications, Anal. Lett. 39 (2006) 2763–2774.